Check for updates

AGU ADVANCING EARTH AND SPACE SCIENCES

Geophysical Research Letters

RESEARCH LETTER
10.1029/2025GL120339

How Fault Zone Fabric Controls the Hydro-Mechanical Behavior and Evolution of Critical State Shearing in Clay Shale

L. Winhausen[1], M. Ziegler[2], and F. Amann[1,3]

[1]Department of Engineering Geology and Hydrogeology, RWTH Aachen University, Aachen, Germany, [2]Swiss Federal Office of Topography (swisstopo), Mont Terri URL, St-Ursanne, Switzerland, [3]Fraunhofer IEG, Aachen, Germany

Key Points:

- Hydro-mechanical coupling of faulted Opalinus Clay from Mont Terri in triaxial shearing experiments
- With increasing effective stress scaly clay transitions from dilative to constant volumetric shearing resulting in critical state conditions
- De-cohesion and pronounced shear strength reduction due to reactivation of multiple tectonic micro shears

Correspondence to:

L. Winhausen,
winhausen@lih.rwth-aachen.de

Citation:

Winhausen, L., Ziegler, M., & Amann, F. (2026). How fault zone fabric controls the hydro-mechanical behavior and evolution of critical state shearing in clay shale. *Geophysical Research Letters*, *53*, e2025GL120339. https://doi.org/10.1029/2025GL120339

Received 29 OCT 2025
Accepted 9 FEB 2026

Author Contributions:

Conceptualization: L. Winhausen, M. Ziegler, F. Amann
Data curation: L. Winhausen
Formal analysis: L. Winhausen
Funding acquisition: L. Winhausen, F. Amann
Investigation: L. Winhausen
Methodology: L. Winhausen
Project administration: L. Winhausen
Visualization: L. Winhausen
Writing – original draft: L. Winhausen
Writing – review & editing: M. Ziegler, F. Amann

© 2026. The Author(s).
This is an open access article under the terms of the Creative Commons Attribution License, which permits use, distribution and reproduction in any medium, provided the original work is properly cited.

Abstract Understanding the hydro-mechanical behavior of faults in clay-rich formations is essential for earthquake mechanics and underground storage applications. We conducted fully hydro-mechanically coupled triaxial tests on preserved fault material from scaly clay sections of the Opalinus Clay formation. The faulted rock exhibits no post-peak weakening and maintains distributed strain accommodation through the reactivation of multiple, sub-parallel tectonic micro-shears. The hydro-mechanical response is stress-dependent, transitioning from dilative shearing at lower effective consolidation stresses to constant volumetric shearing at higher effective consolidation stresses, eventually resulting in critical state conditions. Shear strength analysis revealed the absence of cohesion in the scaly clay fabric, which reduces the rock's shear strength to below the residual strength of the intact rock. These findings provide direct experimental evidence for distributed, steady-state shearing in naturally faulted clay shale and highlight the need to incorporate fabric-dependent behavior into models of fault mechanics.

Plain Language Summary How clay-rich faults deform is key to understanding earthquake processes and subsurface storage applications. We performed fully coupled hydro-mechanical triaxial compression tests on preserved fault material from scaly clay zones in the Opalinus Clay formation. The fault rock did not show post-peak weakening but instead accommodated deformation through distributed slip along several pre-existing sub-parallel micro-shears. The deformation behavior varies with stress: at low effective stress, shearing is dilative, while at higher stresses, deformation occurs at nearly constant volume and evolves toward a critical state, that is, without any stress changes. Our analysis showed that scaly clay has no cohesion and that its shear strength is lower than that of sheared intact rock. The results provide direct experimental evidence for distributed, steady-state shearing in naturally faulted clay-rich rock and highlight the need to incorporate fabric-controlled material properties in fault mechanics models.

1. Introduction

Faults are structural discontinuities in the Earth's subsurface that pose risks to many geoengineering applications, since they constitute mechanical weaknesses, may accommodate large displacements, and alter the rock's hydraulic properties. Knowing the hydro-mechanical behavior of faults and fault zones is important for predicting earthquake mechanics and for assessing seal integrity for fluid storage, such as H_2, CO_2, or for radioactive waste disposal.

Fault zones typically contain a variety of structural elements, whose composition consists of zones of varying rock damage intensity and associated deformation mechanisms. These zones are characterized by varying degrees of strain localization and fabric changes (Faulkner et al., 2010). Hence, the mechanical and hydraulic behavior depends equally on the structural damage within the fault system (Caine et al., 1996). Only a few experimental studies have shown that tectonic structural damage reduces the elasticity and compressive strength of rock (Habimana et al., 2002; Laws et al., 2003) and leads to de-cohesion of the rock (Ikari et al., 2015). Despite the critical importance of understanding coupled hydro-mechanical properties in fault zones for applications such as gas storage and earthquake mechanics, systematic experimental studies remain scarce. This is largely due to the significant challenges associated with preparing representative specimens from natural fault rocks, which hinder direct investigation of how fault damage influences effective geomechanical properties.

Mechanical weakening in fault zones is commonly associated with the presence of fault gouge (e.g., Faulkner et al., 2003), which forms in brittle fault cores where deformation is accommodated by frictional sliding.

Therefore, shear experiments on gouge analogs, typically prepared from powdered materials, are a standard approach for characterizing frictional behavior (see reviews by Marone, 1998; Verberne et al., 2020). These analogs often contain phyllosilicates, which are abundant in natural fault cores and are known to reduce frictional strength, thereby promoting slip along pre-existing zones of weakness (Carpenter et al., 2016; Niemeijer & Spiers, 2005; Tembe et al., 2010). Mineralogical transformations during faulting thus play a key role in controlling fault strength and slip behavior.

For clay shales and similar rocks, the mineralogical contrasts between the fault zone and the surrounding rock may be minimal and ineffective, as both contain high levels of phyllosilicates, that is, clay minerals. Associated differences between the frictional strength of faulted and non-deformed clay shales are therefore hypothesized to be dominated by their structural fabric. Frictional sliding experiments by Collettini et al. (2009) support this hypothesis, showing that natural fault rocks have lower friction coefficients than their powdered analogs.

Fault zones in claystones or shales exhibit various spatial and temporal manifestations of failure at different scales (Aydin, 2014), displaying deformation mechanisms of both brittle and ductile character depending on the geological boundary conditions (e.g., stress, Nygård et al., 2006; Winhausen, Klaver, et al., 2021). A particular feature of fault zones in clayey or shaley formations is the presence of a scaly clay structure, consisting of anastomosing thin, shiny surfaces along which slip has occurred (Agar et al., 1989; Vannucchi, 2019; Vannucchi et al., 2003). Along these thin, penetrative shears, the clay mineral aggregates often display a parallel fabric alignment surrounding undeformed lenses of the protolith. The scaly fabric in clay-dominated soils reduces strength and compressibility compared to their non-fissured analogs (Vitone & Cotecchia, 2011).

The Main Fault intersecting the Opalinus Clay at the Mont Terri Underground Research Laboratory in Switzerland offers a unique opportunity to investigate the influence of fault structures on the hydro-mechanical properties of clay-rich rock. Decades of intensive research have yielded a comprehensive understanding of the intact geomechanical and hydraulic properties of Opalinus Clay (e.g., Gotzen et al., 2025; Schuster et al., 2021; Wild & Amann, 2018; Wild et al., 2015; Winhausen, Klaver, et al., 2021; Winhausen et al., 2023). This well-established baseline makes Opalinus Clay an exceptional natural laboratory for directly comparing the properties of intact host rock with those altered by faulting, offering rare insight into how fault zone structures modify hydro-mechanical behavior in clay-rich rock.

2. Mont Terri's Main Fault

The Main Fault at the Mont Terri Laboratory is a 0.8–3 m thick, SSE-dipping thrust fault in the shaly facies of the Opalinus Clay formation (Figure 1a). Bedding planes and fault zone boundaries have a similar strike (N60°), but the fault zone dips, on average, 15° steeper. The main fault comprises a variety of structural features, such as thin shear bands, slickensides, meso-scale folds, microfolds, an approximately 2-cm-thick gouge layer, and sections rich in scaly clay (Jaeggi et al., 2017; Laurich et al., 2014, 2018; Nussbaum et al., 2011). In the scaly clay sections, multiple microlithons are separated by thin micro-shears, comprising polished surfaces with slickensides indicating fault displacement along these narrow zones. These micron-thin shears are low in porosity and characterized by the preferred alignment of fabric, that is, mainly clay mineral aggregates (Laurich et al., 2017, 2018).

Hydraulic borehole tests conducted at larger intervals (1.4 m) indicate that the fault zone's permeability is controlled by multiple hydraulic pathways rather than a uniform structure. Average permeabilities are low in the order of 10E-20 m^2, in directions sub-perpendicular to the fault plane (Zappone et al., 2021). However, higher-resolution tests using gas as the permeating fluid, in both shorter packer intervals (0.3 m; Kneuker et al., 2017) and on core-scale samples (Wenning et al., 2021), reveal pronounced spatial variability. Localized zones exhibit permeabilities several orders of magnitude higher than those of the intact rock, that is, in the order of 10E-20 to 10E-21 m^2 (Winhausen, Amann-Hildenbrand, et al., 2021; Yu et al., 2017). These results highlight the heterogeneous nature of fluid flow at smaller scales within an otherwise uniformly low-permeability fault zone.

In situ studies have demonstrated the potential for reactivation of fault structures due to induced stress changes resulting from fluid injection experiments (Guglielmi et al., 2020) and during excavation works (Amann et al., 2017; Thoeny, 2014). To improve numerical models simulating the hydro-mechanical response during fault reactivation (e.g., Cappa et al., 2022; Park et al., 2020) or fault-induced damage development around underground openings (Yong et al., 2010; Zhao et al., 2024), the material properties of natural faulted rock must be determined to calibrate constitutive models against experiments on natural fault material.

19448007, 2026, 4, Downloaded from https://agupubs.onlinelibrary.wiley.com/doi/10.1029/2025GL120339 by Universitatsbibliothek RWTH Aachen University, Wiley Online Library on [26/02/2026]. See the Terms and Conditions (https://onlinelibrary.wiley.com/terms-and-conditions) on Wiley Online Library for rules of use; OA articles are governed by the applicable Creative Commons License

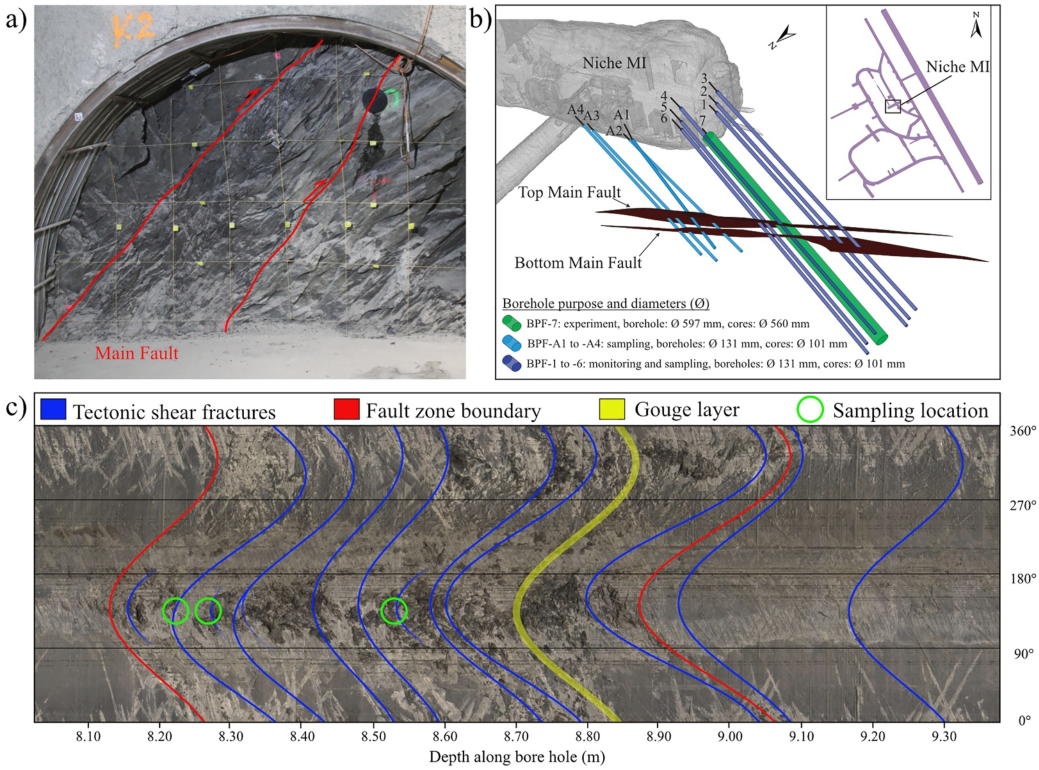

Figure 1. (a) Window in Gallery 98 showing Mont Terri's Main Fault. (b) Location and orientation of the boreholes of the PF/PF-A experiment at the Mont Terri Underground Laboratory. (c) Optical televiewer image from borehole BPF-1 and structural mapping of tectonic features, including sampling locations.

We address this critical knowledge gap by presenting the first fully hydro-mechanically coupled triaxial tests on preserved fault material from the Main Fault in Opalinus Clay at Mont Terri. These tests capture the complete pore pressure response during the pre- and post-failure regimes, offering unprecedented insight into the coupled behavior of natural fault rock. While the primary focus is on capturing the fully coupled hydro-mechanical response, the tests also yield effective strength parameters for the fault material, providing critical input for modeling.

3. Experimental Procedure

Within the scope of the PF-experiment (Ziegler et al., 2025), a 600 mm diameter experimental borehole accompanied by six smaller 131 mm diameter monitoring boreholes was drilled crossing the Main Fault at Mont Terri. Drilling was performed from the MI Niche toward the west at a dip of 10°, creating an intersection angle of approximately 40° with the boundary of the Main Fault (Figure 1b). The cores were obtained by triple-tube core barrel drilling with PVC liners to minimize damage during drilling, and the cores were then air-tight sealed in aluminum bags to obtain the best sample quality and preserve the natural water content.

In this study, we used a core from borehole BPF-1 to prepare specimens for hydro-mechanical testing. The fault core containing the scaly clay was encountered at depths ranging from 8.1 to 8.9 m. Sampling locations were selected based on a very similar structural fabric, that is, within the scaly clay section (Figure 1c), that appeared as a cohesive core piece. Cylindrical specimens measuring 60 mm in length and 30 mm in diameter were prepared by drilling and cutting under dry conditions. The specimens' axes were oriented at an angle of ±10° relative to the orientations of tectonic shear fractures and the scaly clay fabric.

The trimmed endfaces were used to determine the mineralogy based on X-ray diffraction (XRD) measurements of dry powders spiked with an internal standard. Rietveld refinement was applied using the software Profex, which involved custom-made clay mineral structures (Doebelin & Kleeberg, 2015; Ufer et al., 2008, 2015). The cylindrical specimens were weighed before and after the test, followed by oven drying to constant weight at 105°C

19448007, 2026, 4, Downloaded from https://agupubs.onlinelibrary.wiley.com/doi/10.1029/2025GL120339 by Universitatsbibliothek RWTH Aachen University, Wiley Online Library on [26/02/2026]. See the Terms and Conditions (https://onlinelibrary.wiley.com/terms-and-conditions) on Wiley Online Library for rules of use; OA articles are governed by the applicable Creative Commons License

19448007, 2026, 4, Downloaded from https://agupubs.onlinelibrary.wiley.com/doi/10.1029/2025GL120339 by Universitatsbibliothek RWTH Aachen University, Wiley Online Library on [26/02/2026]. See the Terms and Conditions (https://onlinelibrary.wiley.com/terms-and-conditions) on Wiley Online Library for rules of use; OA articles are governed by the applicable Creative Commons License

to measure their water content. A scanning electron microscope was used to investigate the microstructure of ion beam-polished sections cut from the trimmed endfaces and the tested specimens.

Triaxial tests were conducted using a servo-electric axial load frame and a pressure vessel operable using oil as the confining pressure medium. The specimens were back-saturated with artificial pore water at their top and bottom endfaces. A detailed description of the testing apparatus was presented by Winhausen et al. (2022). The testing protocol consisted of a saturation phase, including checks for Skempton's B-coefficient, a consolidation phase, and the final shearing phase (see Winhausen et al., 2022, for further details). The shearing phase was conducted at constant axial strain rates ranging from 1.22E-7 to 7.04E-08 s^{-1}. These rates were estimated based on the consolidation coefficient obtained for each specimen and the time required for pore water pressure equilibration within the specimen. The tests were terminated once the stress state reached quasi steady-state conditions. Tests were conducted with effective confinements of 4 MPa (SC4), 10 MPa (SC10) and 16 MPa (SC16).

We compare our results to those obtained from tests performed on intact Opalinus Clay from Mont Terri. These tests were carried out on the same formation, that is, the shaly facies, and using the same experimental procedure and equal boundary conditions (Winhausen et al., 2022).

4. Specimen Characterization

The XRD measurements showed that the specimens tested are very similar in terms of their mineralogy (for details see data of Winhausen, 2026). The scaly clay is dominated by clay minerals, accounting for approximately two thirds of the total, with the largest shares being muscovite/illite and kaolinite/chlorite, at on average, 21 and 26 wt% each, and the remaining average 15 wt% mixed-layer clay minerals. The other main constituents are calcite and quartz, at each at around 11–12 wt%, and feldspar (albite and microcline) at around 7 wt%. Accessory minerals such as pyrite, siderite, and anatase have a total share of approximately 5 wt%. Our XRD data show that the mineralogical composition of scaly clay from the Main Fault is comparable to that of the intact shaly formation, which is characterized by similar proportions of mineral constituents (e.g., Pearson et al., 2003). The similarity of the mineralogy of scaly clay and intact Opalinus Clay from Mont Terri has also been reported in the literature (Clauer et al., 2025; Kneuker et al., 2017; Laurich et al., 2018). The gravimetric water contents of the specimens before testing were 7.27%–8.23%, while they were 8.25%–8.95% after testing. These values are only slightly larger than those of intact specimens (7.2%–7.5% on average; e.g., Amann et al., 2011; Winhausen, Amann-Hildenbrand, et al., 2021) and prove proper core preservation. In conclusion, we attribute changes in the hydromechanical behavior solely to the structural nature, as neither the mineralogy nor the water content exhibits significant differences between tectonically disturbed and undisturbed Opalinus Clay.

5. Results and Discussion

5.1. Hydro-Mechanical Coupling

The hydro-mechanical response under undrained triaxial compression is analyzed based on the stress-strain behavior and the development of excess pore water pressure until axial strains of 3%–4% are reached. Figure 2a shows the evolution of axial and radial strains for specimens consolidated at effective stresses of 4, 10, and 16 MPa. All samples exhibit strain-hardening behavior, with initially high hardening rates that progressively decrease toward a quasi steady-state condition. This quasi steady-state was reached at axial strains of approximately 0.6% (SC4, SC10) to 1.5% (SC16), corresponding to differential stresses of 3, 6, and 12 MPa, respectively. Undrained elastic moduli were determined as tangent moduli within the early loading phase, up to differential stresses of 0.28 MPa (SC4) and 0.5 MPa (SC10, SC16). Young's moduli were 2.6, 4.0, and 7.3 GPa, whereas Poisson's ratios normal to the bedding orientation yielded values ranging between 0.5 and 0.6. The excess pore water pressure exhibited a similar response during deviatoric loading (Figure 2c): It initially increased, then developed into a plateau or decreased slightly. An exception is the test conducted at 4 MPa effective confinement, where the excess pore water pressure continuously decreased after reaching its maximum of 0.53 MPa.

The hydro-mechanical behavior of the scaly clay differs markedly from that of structurally intact Opalinus Clay. As shown in Figure 2c and in previous studies (see Winhausen et al., 2022), intact specimens exhibit strain hardening up to a distinct peak stress, followed by a pronounced strain softening phase associated with a brittle post-failure stress drop. This behavior is characteristic of overconsolidated clay shales under comparable effective stress conditions (Ewy et al., 2020; Islam & Skalle, 2013). In contrast, the scaly clay shows continuous hardening

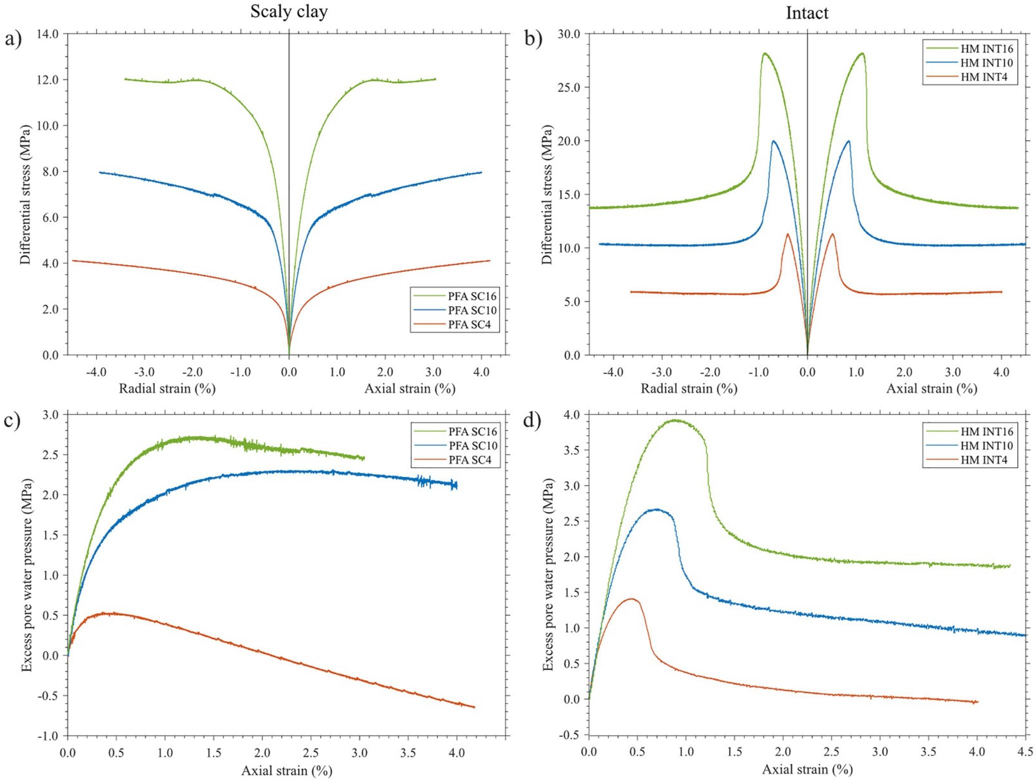

Figure 2. Stress-strain and excess pore water pressure development for scaly clay (a, c) and intact (b, d) Opalinus Clay. Data for tests on intact rock specimens from Winhausen et al. (2022). The hydro-mechanical response of scaly clay shows continuous strain-hardening. It is stress-dependent, transitioning from dilatant shearing at lower effective consolidation stresses to constant volumetric shearing at higher effective consolidation stresses, eventually leading to critical state conditions.

throughout the test, without a clear peak or post-peak weakening, even at axial strains exceeding 4%. Similarly, the excess pore pressure response differs: Intact samples develop a sharp pore pressure peak, followed by a reduction to a lower steady-state level. In contrast, the scaly clay exhibit a gradual increase that stabilizes at a higher ultimate value, particularly at consolidation stresses of 10 and 16 MPa.

One of the most striking observations from the scaly clay tests is the pore pressure response, which reveals two distinct deformation regimes. At low effective consolidation stress (≤4 MPa), the specimens exhibit persistent dilatancy, resulting in a continuous decrease in pore pressure well below the initial value (Figure 2c). In contrast, at higher effective stresses (≥10 MPa), deformation is purely compactive, with pore pressure steadily increasing and stabilizing at elevated levels. While a transition from dilative to less dilative behavior with increasing stress has been reported for intact Opalinus Clay under deviatoric loading (Amann et al., 2012; Winhausen et al., 2022, 2023), the complete suppression of dilatancy observed here is unique to the faulted rock material from Mont Terri. Notably, intact samples display only transient instead of continuous dilatancy immediately post-peak, followed by the development of relatively stable excess pore pressure, highlighting a fundamental difference in hydro-mechanical behavior between intact and faulted Opalinus Clay.

A key finding of this study is the hydro-mechanical coupling behavior of scaly clay Opalinus Clay under deviatoric loading, which is best understood in terms of its effective stress evolution. As shown in Figure 3, all specimens initially exhibit a phase of nearly constant mean effective stress during shearing, implying minimal volumetric strain. Beyond this initial phase, the response diverges depending on the effective consolidation stress. At the lowest confinement (4 MPa), the effective stress path begins to rise steadily with a quasi linear slope, indicating persistent dilation. The continued expansion of pore volume beyond the initial state suggests ongoing shear-induced dilatancy, characteristic of materials undergoing strain hardening in a dilative regime. In contrast, specimens consolidated at 10 and 16 MPa exhibit effective stress paths that converge toward a constant p′–q state,

19448007, 2026, 4, Downloaded from https://agupubs.onlinelibrary.wiley.com/doi/10.1029/2025GL120339 by Universitatsbibliothek RWTH Aachen University, Wiley Online Library on [26/02/2026]. See the Terms and Conditions (https://onlinelibrary.wiley.com/terms-and-conditions) on Wiley Online Library for rules of use; OA articles are governed by the applicable Creative Commons License

10.1029/2025GL120339

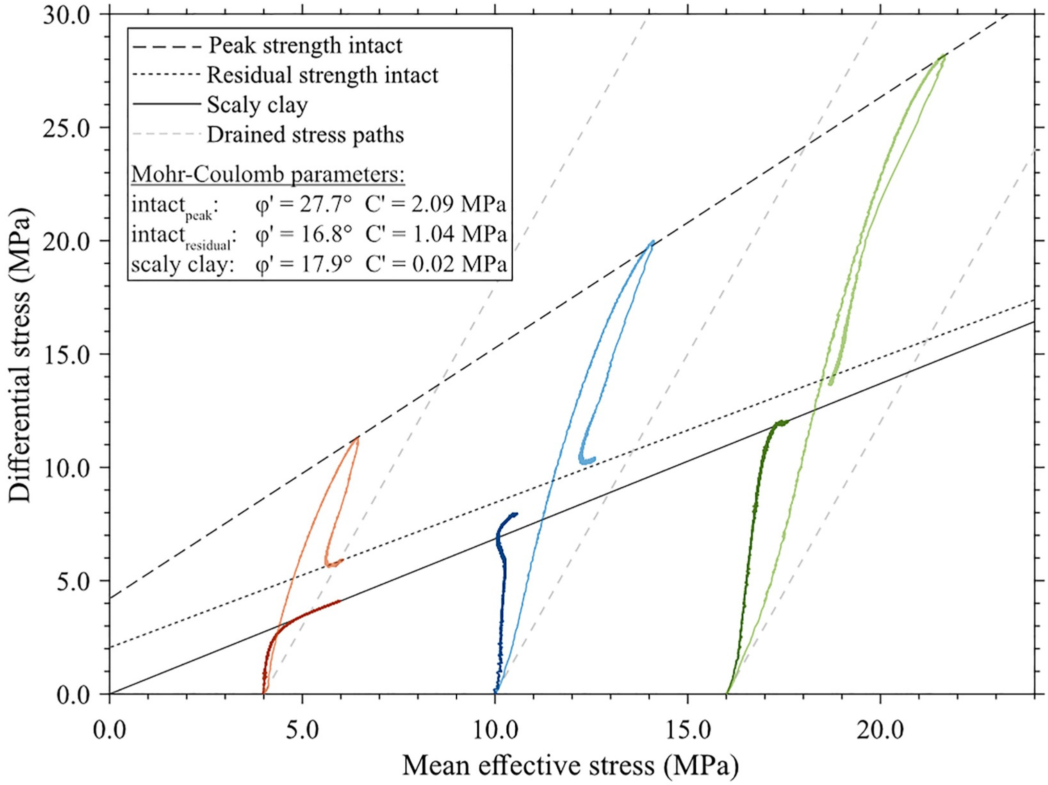

Figure 3. Effective stress paths for intact (light colored lines) and scaly clay (dark colored lines) specimens. Black lines represent Mohr-Coulomb shear strength envelopes with fitting parameters ϕ' and C'. Scaly clay has almost zero cohesion and reduces the shear strength of Opalinus Clay below that of the intact rock.

with no further evolution during continued shearing. This behavior is indicative of steady-state deformation under iso-choric, that is, constant-volume, conditions, which is commonly associated with the critical state, a condition in which the material flows plastically without further volumetric or stress changes.

The approach to critical state behavior is characteristic of low-cohesion or structured soils and indicates that, at higher confining pressures, the faulted Opalinus Clay behaves more like a reworked granular material than an intact rock. These observations not only provide direct experimental evidence for critical state conditions in natural fault rock and gouge but also highlight the stress-dependent transition between dilative hardening and steady-state shearing. This has implications for fault stability, fluid pressure evolution, and deformation localization in clay-rich fault zones.

5.2. Effective Strength

The shear strength envelopes derived from the three tests (Figure 3) were evaluated using a Mohr-Coulomb framework in p′–q space, using a least squares regression method. While it is expected that faulted material exhibits reduced strength, a notable finding is that the scaly clay specimens fall below the residual strength envelope of intact Opalinus Clay. This indicates that fault-related fabric changes reduce the shear strength, which is not only lower than the peak strength of intact rock but also significantly weaker than its post-failure residual strength. This difference is primarily due to a marked reduction in cohesion; both materials exhibit only minor differences in residual friction angles (17.9° and 16.8° for the scaly clay and intact rock, respectively). Yet, the tectonically faulted rock has effectively zero cohesion (0.02 MPa), compared to 1.04 MPa for the intact material. This highlights the fact that tectonic fabric and associated microstructural reworking in fault zones can drastically reduce the effective strength of clay shales, even beyond what is observed after large-strain failure in intact specimens.

19448007, 2026, 4, Downloaded from https://agupubs.onlinelibrary.wiley.com/doi/10.1029/2025GL120339 by Universitatsbibliothek RWTH Aachen University, Wiley Online Library on [26/02/2026]. See the Terms and Conditions (https://onlinelibrary.wiley.com/terms-and-conditions) on Wiley Online Library for rules of use; OA articles are governed by the applicable Creative Commons License

19448007, 2026, 4, Downloaded from https://agupubs.onlinelibrary.wiley.com/doi/10.1029/2025GL120339 by Universitatsbibliothek RWTH Aachen University, Wiley Online Library on [26/02/2026]. See the Terms and Conditions (https://onlinelibrary.wiley.com/terms-and-conditions) on Wiley Online Library for rules of use; OA articles are governed by the applicable Creative Commons License

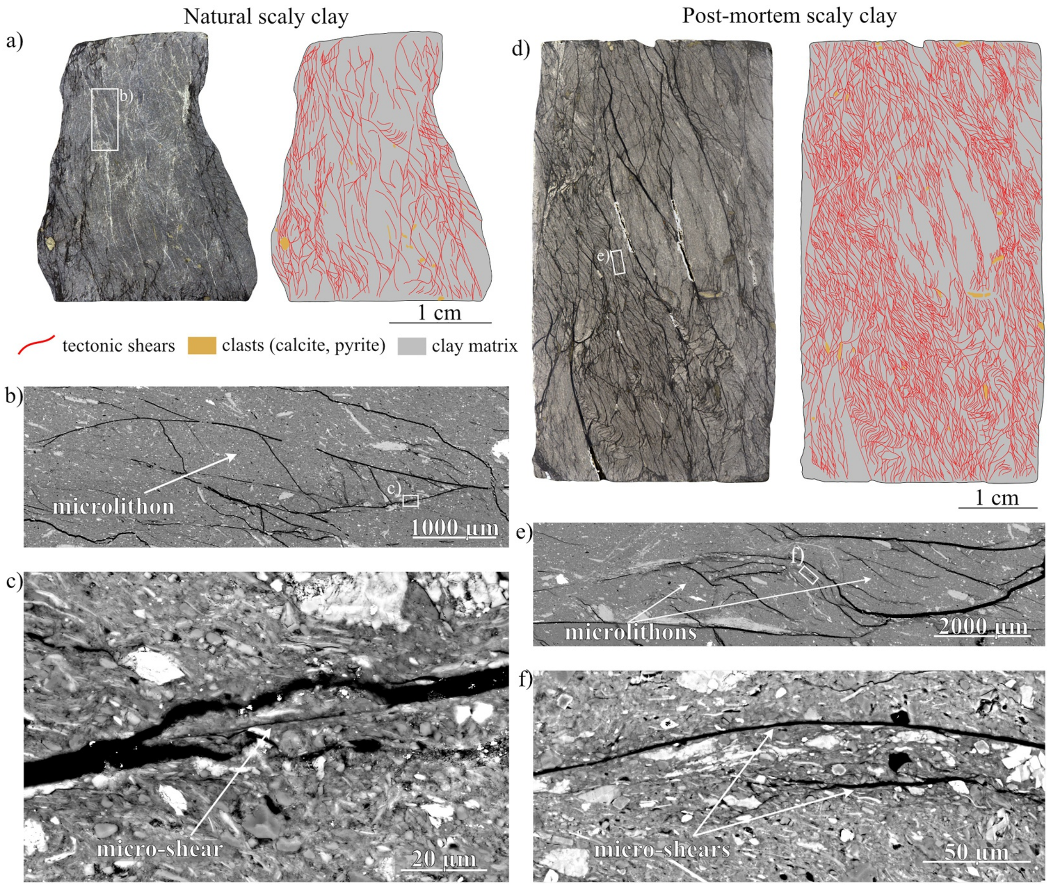

Figure 4. Structural appearance of scaly clay before ("natural scaly clay," a–c) and after experimental shear deformation ("post-mortem," d–f). Panel (d) presents the cut surface along the vertical axis of the entire specimen SC4. Microstructure before and after laboratory deformation shows microlithons separated by thin micro-shears. The similarity of the microstructural fabrics suggests that pre-existing tectonic shears were reactivated during the experiment.

Although the scaly clay was recovered as apparently intact and cohesive core material, this does not contradict its effectively zero cohesion under saturated, drained conditions. The apparent strength is likely due to suction pressures that develop upon undrained unloading during drilling. These negative pore pressures temporarily create tensile strength to the material, giving it the appearance of cohesion. This mechanism is consistent with findings on absolute negative pore pressures in low-permeability rocks (e.g., Khaledi et al., 2021).

5.3. Failure Localization

The microstructure of natural scaly clay reveals multiple shear bands of varying widths oriented around lenses of relatively undeformed microlithons. These abundant tectonic shears are characterized by a preferred fabric orientation and polished surfaces with marginal cohesive bonding. These micro-shears form a scaly fabric organized as an anastomosing network surrounding elongated, undeformed rock lenses and are locally arranged as microfolds.

Triaxial deformation produced multiple shear planes oriented sub-parallel to the specimen axis (Figure 4b). In contrast to the highly localized failure typical of intact Opalinus Clay (Gotzen et al., 2025; Schuster et al., 2021; Winhausen, Klaver, et al., 2021), no single inclined shear plane was identified. Instead, deformation resulted in a dense network of micro-shears that structurally resemble the pristine fault microstructure (Figure 4a, see also Laurich et al., 2017, 2018). The well-polished tectonic shear surfaces, characterized by the shape-preferred orientation of clay aggregates, are low in frictional resistance due to the absence of asperities (Figure 4) and therefore, favor local sliding. Thus, shear failure is manifested by the reactivation of pre-existing tectonic micro-scale shear planes and localized slip distributed within the entire specimen.

19448007, 2026, 4, Downloaded from https://agupubs.onlinelibrary.wiley.com/doi/10.1029/2025GL120339 by Universitatsbibliothek RWTH Aachen University, Wiley Online Library on [26/02/2026]. See the Terms and Conditions (https://onlinelibrary.wiley.com/terms-and-conditions) on Wiley Online Library for rules of use; OA articles are governed by the applicable Creative Commons License

Together with the poromechanical response of the specimens, these findings suggest that deformation was accommodated simultaneously along multiple micro-shear surfaces. This interpretation is consistent with previous deformation experiments on scaly clay analogs documenting distributed slip along anastomosing shear networks (Tarling & Rowe, 2016).

Once plastic shear strain develops, two distinct deformation modes arise. At lower effective stresses, the scaly fabric deforms in a hybrid, dilatant mode where local detachment between microlithons produces volumetric expansion. Effective stresses above ≥10 MPa are sufficient to inhibit this detachment, leading to non-dilative frictional sliding under near-pure shear conditions without bulk volume change.

The dense network of tectonic shears forming the scaly fabric exerts a first-order control on the hydromechanical behavior of Opalinus Clay. Although shearing of intact Opalinus Clay experimentally to large strains produces slickensides and microscale shear zones, the residual shear strength remains higher than that of naturally faulted OPA. The abundance, geometry, and connectivity of the scaly fabric therefore play a key role in governing both poromechanical response and bulk strength. We suggest that this fault behavior applies not only to clay-rich rocks but also to fault rocks that structurally resemble scaly clay, specifically those that contain a relatively dense network of thin tectonic micro-shears.

6. Conclusions

Hydro-mechanically coupled, undrained triaxial tests on faulted clay shale reveal that the poromechanical behavior is highly influenced by the rock fabric, that is, scaly clay. The scaly fabric causes continuous strain hardening and shows a stress-dependent transition from dilatant, hybrid shearing at low effective stresses (≤4 MPa) to constant volumetric, steady-state deformation at higher stresses (≥10 MPa), resulting in critical state shearing. The shear strength analysis indicates the absence of cohesion in the fault-related scaly clay fabric, resulting in shear strengths below the residual envelope of the intact rock material.

Microstructural observations confirm that deformation occurs through the distributed reactivation of preexisting tectonic micro-shears enclosing undeformed microlithons.

Our experimental data suggest that natural clay-rich faults are more likely to exhibit stable, aseismic creep rather than sudden, unstable rupture. This interpretation is primarily rooted in the observed absence of post-peak weakening; unlike intact rock, which typically exhibits a pronounced brittle stress drop, scaly clay demonstrates continuous strain-hardening. This lack of weakening suggests that the material does not easily transition into the "velocity-weakening" behavior typically associated with earthquake nucleation. Furthermore, our study suggests that deformation is not localized on a single plane but is instead distributed across a dense network of reactivated tectonic micro-shears. Our study demonstrates that inherited fault fabric exerts first-order control on the coupled hydro-mechanical response of clay shales, and potentially other fault rock, emphasizing the importance of incorporating fabric-dependent behavior in models of fault stability.

Conflict of Interest

The authors declare no conflicts of interest relevant to this study.

Data Availability Statement

The data (Winhausen, 2026) obtained from mineralogical analysis and triaxial testing are available at https://doi.org/10.17605/OSF.IO/T85JA.

Acknowledgments
We would like to thank the Mont Terri consortium for funding the PF-A experiment. We acknowledge the help of Timo Seemann (RWTH Aachen University) for performing the XRD measurements and Caroline Etter (swisstopo) for providing input to Figure 1. Ben Laurich (BGR) is thanked for the fruitful discussions of the results. Finally, we would like to thank the anonymous reviewer and Alba Zappone (ETH Zürich) for their comments and suggestions, which improved the quality of this work. Open Access funding enabled and organized by Projekt DEAL.

References

Agar, S. M., Prior, D. J., & Behrmann, J. H. (1989). Back-scattered electron imagery of the tectonic fabrics of some fine-grained sediments: Implications for fabric nomenclature and deformation processes. *Geology*, *17*(10), 901–904. https://doi.org/10.1130/0091-7613(1989)017<0901:bseiot>2.3.co;2

Amann, F., Button, E. A., Evans, K. F., Gischig, V. S., & Blümel, M. (2011). Experimental study of the brittle behavior of clay shale in rapid unconfined compression. *Rock Mechanics and Rock Engineering*, *44*(4), 415–430. https://doi.org/10.2139/ssrn.5429158

Amann, F., Kaiser, P., & Button, E. A. (2012). Experimental study of brittle behavior of clay shale in rapid triaxial compression. *Rock Mechanics and Rock Engineering*, *45*(1), 21–33. https://doi.org/10.1007/s00603-011-0195-9

Amann, F., Wild, K. M., Loew, S., Yong, S., Thoeny, R., & Frank, E. (2017). Geomechanical behaviour of Opalinus Clay at multiple scales: Results from Mont Terri rock laboratory (Switzerland). In *Mont Terri rock laboratory, 20 years: Two decades of research and experimentation on claystones for geological disposal of radioactive waste* (pp. 153–173). Springer.

Aydin, A. (2014). Failure modes of shales and their implications for natural and man-made fracture assemblages. *AAPG Bulletin*, *98*(11), 2391–2409. https://doi.org/10.1306/07311413112

Caine, J. S., Evans, J. P., & Forster, C. B. (1996). Fault zone architecture and permeability structure. *Geology*, *24*(11), 1025–1028. https://doi.org/10.1130/0091-7613(1996)024<1025:fzaaps>2.3.co;2

Cappa, F., Guglielmi, Y., Nussbaum, C., De Barros, L., & Birkholzer, J. (2022). Fluid migration in low-permeability faults driven by decoupling of fault slip and opening. *Nature Geoscience*, *15*(9), 747–751. https://doi.org/10.1038/s41561-022-00993-4

Carpenter, B. M., Ikari, M. J., & Marone, C. (2016). Laboratory observations of time-dependent frictional strengthening and stress relaxation in natural and synthetic fault gouges. *Journal of Geophysical Research: Solid Earth*, *121*(2), 1183–1201. https://doi.org/10.1002/2015jb012136

Clauer, N., Nussbaum, C., Boiron, M.-C., & Ulrich, M. (2025). Chemical tracing and isotopic dating of authigenic illite-type minerals in centimeter-sized gouges of the "Main Fault" within the Opalinus Clay (Switzerland). *Clays and Clay Minerals*, *73*, e16. https://doi.org/10.1017/cmn.2024.40

Collettini, C., Niemeijer, A., Viti, C., & Marone, C. (2009). Fault zone fabric and fault weakness. *Nature*, *462*(7275), 907–910. https://doi.org/10.1038/nature08585

Doebelin, N., & Kleeberg, R. (2015). Profex: A graphical user interface for the Rietveld refinement program BGMN. *Applied Crystallography*, *48*(5), 1573–1580. https://doi.org/10.1107/s1600576715014685

Ewy, R., Dirkzwager, J., & Bovberg, C. (2020). Claystone porosity and mechanical behavior vs. geologic burial stress. *Marine and Petroleum Geology*, *121*, 104563. https://doi.org/10.1016/j.marpetgeo.2020.104563

Faulkner, D., Jackson, C., Lunn, R., Schlische, R., Shipton, Z., Wibberley, C., & Withjack, M. (2010). A review of recent developments concerning the structure, mechanics and fluid flow properties of fault zones. *Journal of Structural Geology*, *32*(11), 1557–1575. https://doi.org/10.1016/j.jsg.2010.06.009

Faulkner, D., Lewis, A., & Rutter, E. (2003). On the internal structure and mechanics of large strike-slip fault zones: Field observations of the Carboneras fault in southeastern Spain. *Tectonophysics*, *367*(3–4), 235–251. https://doi.org/10.1016/s0040-1951(03)00134-3

Gotzen, L., Winhausen, L., Jalali, M., Khaledi, K., & Amann, F. (2025). The long-term strength and creep behavior of fully saturated shaly Opalinus Clay. *Engineering Geology*, *348*, 107961. https://doi.org/10.1016/j.enggeo.2025.107961

Guglielmi, Y., Nussbaum, C., Jeanne, P., Rutqvist, J., Cappa, F., & Birkholzer, J. (2020). Complexity of fault rupture and fluid leakage in shale: Insights from a controlled fault activation experiment. *Journal of Geophysical Research: Solid Earth*, *125*(2), e2019JB017781. https://doi.org/10.1029/2019jb017781

Habimana, J., Labiouse, V., & Descoeudres, F. (2002). Geomechanical characterisation of cataclastic rocks: Experience from the Cleuson–Dixence project. *International Journal of Rock Mechanics and Mining Sciences*, *39*(6), 677–693. https://doi.org/10.1016/s1365-1609(02)00042-4

Ikari, M. J., Kameda, J., Saffer, D. M., & Kopf, A. J. (2015). Strength characteristics of Japan Trench borehole samples in the high-slip region of the 2011 Tohoku-Oki earthquake. *Earth and Planetary Science Letters*, *412*, 35–41. https://doi.org/10.1016/j.epsl.2014.12.014

Islam, M. A., & Skalle, P. (2013). An experimental investigation of shale mechanical properties through drained and undrained test mechanisms. *Rock Mechanics and Rock Engineering*, *46*(6), 1391–1413. https://doi.org/10.1007/s00603-013-0377-8

Jaeggi, D., Laurich, B., Nussbaum, C., Schuster, K., & Connolly, P. (2017). Tectonic structure of the "Main Fault" in the Opalinus Clay, Mont Terri rock laboratory (Switzerland). In *Mont Terri rock laboratory, 20 years: Two decades of research and experimentation on claystones for geological disposal of radioactive waste* (pp. 69–86). Springer.

Khaledi, K., Hamdi, P., Winhausen, L., Jalali, M., Jaeggi, D., & Amann, F. (2021). Unloading induced absolute negative pore pressures in a low permeable clay shale. *Engineering Geology*, *295*, 106451. https://doi.org/10.1016/j.enggeo.2021.106451

Kneuker, T., Hammer, J., Shao, H., Schuster, K., Furche, M., & Zulauf, G. (2017). Microstructure and composition of brittle faults in claystones of the Mont Terri rock laboratory (Switzerland): New data from petrographic studies, geophysical borehole logging and permeability tests. *Engineering Geology*, *231*, 139–156. https://doi.org/10.1016/j.enggeo.2017.10.016

Laurich, B., Urai, J. L., Desbois, G., Vollmer, C., & Nussbaum, C. (2014). Microstructural evolution of an incipient fault zone in Opalinus Clay: Insights from an optical and electron microscopic study of ion-beam polished samples from the main fault in the Mt-Terri underground research laboratory. *Journal of Structural Geology*, *67*, 107–128. https://doi.org/10.1016/j.jsg.2014.07.014

Laurich, B., Urai, J. L., & Nussbaum, C. (2017). Microstructures and deformation mechanisms in Opalinus Clay: Insights from scaly clay from the Main Fault in the Mont Terri rock laboratory (CH). *Solid Earth*, *8*(1), 27–44. https://doi.org/10.5194/se-8-27-2017

Laurich, B., Urai, J. L., Vollmer, C., & Nussbaum, C. (2018). Deformation mechanisms and evolution of the microstructure of gouge in the Main Fault in Opalinus Clay in the Mont Terri rock laboratory (CH). *Solid Earth*, *9*(1), 1–24. https://doi.org/10.5194/se-9-1-2018

Laws, S., Eberhardt, E., Loew, S., & Descoeudres, F. (2003). Geomechanical properties of shear zones in the Eastern Aar Massif, Switzerland and their implication on tunnelling. *Rock Mechanics and Rock Engineering*, *36*(4), 271–303. https://doi.org/10.1007/s00603-003-0050-8

Marone, C. (1998). Laboratory-derived friction laws and their application to seismic faulting. *Annual Review of Earth and Planetary Sciences*, *26*(1), 643–696. https://doi.org/10.1146/annurev.earth.26.1.643

Niemeijer, A. R., & Spiers, C. J. (2005). Influence of phyllosilicates on fault strength in the brittle-ductile transition: Insights from rock analogue experiments. In D. Bruhn, & L. Burlini (Eds.), *High-strain zones: Structure and physical properties* (Vol. 245, pp. 303–327). https://doi.org/10.1144/gsl.sp.2005.245.01.15

Nussbaum, C., Bossart, P., Amann, F., & Aubourg, C. (2011). Analysis of tectonic structures and excavation induced fractures in the Opalinus Clay, Mont Terri underground rock laboratory (Switzerland). *Swiss Journal of Geosciences*, *104*(2), 187–210. https://doi.org/10.1007/s00015-011-0070-4

Nygård, R., Gutierrez, M., Bratli, R. K., & Høeg, K. (2006). Brittle–ductile transition, shear failure and leakage in shales and mudrocks. *Marine and Petroleum Geology*, *23*(2), 201–212.

Park, J.-W., Guglielmi, Y., Graupner, B., Rutqvist, J., Kim, T., Park, E.-S., & Lee, C. (2020). Modeling of fluid injection-induced fault reactivation using coupled fluid flow and mechanical interface model. *International Journal of Rock Mechanics and Mining Sciences*, *132*, 104373. https://doi.org/10.1016/j.ijrmms.2020.104373

Pearson, F., Arcos, D., Bath, A., Boisson, J., Fernández, A., Gäbler, H., et al. (2003). *Mont Terri project-geochemistry of water in the Opalinus Clay formation at the Mont Terri rock laboratory* (Vol. 5). Office fédéral des eaux et de la géologie OFEG.

Schuster, V., Rybacki, E., Bonnelye, A., Herrmann, J., Schleicher, A. M., & Dresen, G. (2021). Experimental deformation of Opalinus Clay at elevated temperature and pressure conditions: Mechanical properties and the influence of rock fabric. *Rock Mechanics and Rock Engineering*, *54*(8), 4009–4039. https://doi.org/10.1007/s00603-021-02474-3

Tarling, M. S., & Rowe, C. D. (2016). Experimental slip distribution in lentils as an analog for scaly clay fabrics. *Geology*, *44*(3), 183–186. https://doi.org/10.1130/g37306.1

19448007, 2026, 4, Downloaded from https://agupubs.onlinelibrary.wiley.com/doi/10.1029/2025GL120339 by Universitatsbibliothek RWTH Aachen University, Wiley Online Library on [26/02/2026]. See the Terms and Conditions (https://onlinelibrary.wiley.com/terms-and-conditions) on Wiley Online Library for rules of use; OA articles are governed by the applicable Creative Commons License

Tembe, S., Lockner, D. A., & Wong, T.-F. (2010). Effect of clay content and mineralogy on frictional sliding behavior of simulated gouges: Binary and ternary mixtures of quartz, illite, and montmorillonite. *Journal of Geophysical Research*, *115*(B3), B03416. https://doi.org/10.1029/2009jb006383

Thoeny, R. (2014). *Geomechanical analysis of excavation-induced rock mass behavior of faulted Opalinus Clay at the Mont Terri underground rock laboratory (Switzerland)* (Published doctoral dissertation). Swiss Federal Institute of Technology. https://doi.org/10.3929/ethz-a-010174753

Ufer, K., Kleeberg, R., & Monecke, T. (2015). Quantification of stacking disordered Si–Al layer silicates by the Rietveld method: Application to exploration for high-sulphidation epithermal gold deposits. *Powder Diffraction*, *30*(S1), S111–S118. https://doi.org/10.1017/s0885715615000111

Ufer, K., Stanjek, H., Roth, G., Dohrmann, R., Kleeberg, R., & Kaufhold, S. (2008). Quantitative phase analysis of bentonites by the Rietveld method. *Clays and Clay Minerals*, *56*(2), 272–282. https://doi.org/10.1346/ccmn.2008.0560210

Vannucchi, P. (2019). Scaly fabric and slip within fault zones. *Geosphere*, *15*(2), 342–356. https://doi.org/10.1130/ges01651.1

Vannucchi, P., Maltman, A., Bettelli, G., & Clennell, B. (2003). On the nature of scaly fabric and scaly clay. *Journal of Structural Geology*, *25*(5), 673–688. https://doi.org/10.1016/s0191-8141(02)00066-4

Verberne, B. A., Van Den Ende, M., Chen, J., Niemeijer, A. R., & Spiers, C. J. (2020). The physics of fault friction: Insights from experiments on simulated gouges at low shearing velocities. *Solid Earth*, *11*(6), 2075–2095. https://doi.org/10.5194/se-11-2075-2020

Vitone, C., & Cotecchia, F. (2011). The influence of intense fissuring on the mechanical behaviour of clays. *Géotechnique*, *61*(12), 1003–1018. https://doi.org/10.1680/geot.9.p.005

Wenning, Q. C., Madonna, C., Zappone, A., Grab, M., Rinaldi, A. P., Plötze, M., et al. (2021). Shale fault zone structure and stress dependent anisotropic permeability and seismic velocity properties (Opalinus Clay, Switzerland). *Journal of Structural Geology*, *144*, 104273. https://doi.org/10.1016/j.jsg.2020.104273

Wild, K. M., & Amann, F. (2018). Experimental study of the hydro-mechanical response of Opalinus Clay–part 1: Pore pressure response and effective geomechanical properties under consideration of confinement and anisotropy. *Engineering Geology*, *237*, 32–41. https://doi.org/10.1016/j.enggeo.2018.02.012

Wild, K. M., Wymann, L. P., Zimmer, S., Thoeny, R., & Amann, F. (2015). Water retention characteristics and state-dependent mechanical and petro-physical properties of a clay shale. *Rock Mechanics and Rock Engineering*, *48*(2), 427–439. https://doi.org/10.1007/s00603-014-0565-1

Winhausen, L. (2026). How fault zone fabric controls the hydro-mechanical behavior and evolution of critical state shearing in clay shale [Dataset]. *OSF*. https://doi.org/10.17605/OSF.IO/T85JA

Winhausen, L., Amann-Hildenbrand, A., Fink, R., Jalali, M., Khaledi, K., Hamdi, P., et al. (2021). A comparative study on methods for determining the hydraulic properties of a clay shale. *Geophysical Journal International*, *224*(3), 1523–1539. https://doi.org/10.1093/gji/ggaa532

Winhausen, L., Khaledi, K., Jalali, M., Bretthauer, M., & Amann, F. (2023). The anisotropic behavior of a clay shale: Strength, hydro-mechanical couplings and failure processes. *Journal of Geophysical Research: Solid Earth*, *128*(11), e2023JB027382. https://doi.org/10.1029/2023jb027382

Winhausen, L., Khaledi, K., Jalali, M., Urai, J. L., & Amann, F. (2022). Failure mode transition in Opalinus Clay: A hydro-mechanical and microstructural perspective. *Solid Earth Discussions*, *2022*(5), 1–26. https://doi.org/10.5194/se-13-901-2022

Winhausen, L., Klaver, J., Schmatz, J., Desbois, G., Urai, J. L., Amann, F., & Nussbaum, C. (2021). Micromechanisms leading to shear failure of Opalinus Clay in a triaxial test: A high-resolution BIB–SEM study. *Solid Earth*, *12*(9), 2109–2126. https://doi.org/10.5194/se-12-2109-2021

Yong, S., Kaiser, P. K., & Loew, S. (2010). Influence of tectonic shears on tunnel-induced fracturing. *International Journal of Rock Mechanics and Mining Sciences*, *47*(6), 894–907. https://doi.org/10.1016/j.ijrmms.2010.05.009

Yu, C., Matray, J.-M., Gonçalvès, J., Jaeggi, D., Gräsle, W., Wieczorek, K., et al. (2017). Comparative study of methods to estimate hydraulic parameters in the hydraulically undisturbed Opalinus Clay (Switzerland). In *Mont Terri rock laboratory, 20 years: Two decades of research and experimentation on claystones for geological disposal of radioactive waste* (pp. 87–106). Springer.

Zappone, A., Rinaldi, A. P., Grab, M., Wenning, Q. C., Roques, C., Madonna, C., et al. (2021). Fault sealing and caprock integrity for co 2 storage: An in situ injection experiment. *Solid Earth*, *12*(2), 319–343. https://doi.org/10.5194/se-12-319-2021

Zhao, C., Lei, Q., Ziegler, M., & Loew, S. (2024). Structurally-controlled failure and damage around an opening in faulted Opalinus Clay shale at the Mont Terri rock laboratory: In-situ experimental observation and 3D numerical simulation. *International Journal of Rock Mechanics and Mining Sciences*, *180*, 105812. https://doi.org/10.1016/j.ijrmms.2024.105812

Ziegler, M., Wang, R., & Loew, S. (2025). Progressive failure of a circular excavation drilled through faulted clay shale—Experimental setup, rock mass structures and damage evolution at excavation boundary. Available at SSRN 5429158.

19448007, 2026, 4, Downloaded from https://agupubs.onlinelibrary.wiley.com/doi/10.1029/2025GL120339 by Universitätsbibliothek RWTH Aachen University, Wiley Online Library on [26/02/2026]. See the Terms and Conditions (https://onlinelibrary.wiley.com/terms-and-conditions) on Wiley Online Library for rules of use; OA articles are governed by the applicable Creative Commons License